BREFCOR – TOWARDS OPERATIONAL BRDF CORRECTION FOR IMAGING SPECTROMETRY DATA

Tal Feingersh [a] Daniel Schläpfer [b], Eyal Ben-Dor [a]

[a] University of Tel-Aviv, Department of Geography and the Human Environment, Tel-Aviv, Israel;
{ftal@post.tau.ac.il, bendor@post.tau.ac.il}
[b] ReSe Applications Schläpfer, Wil, Switzerland; daniel@rese.ch

ABSTRACT

This work is based on the method suggested for correction of reflectance anisotropy in imaging spectroscopy data, outlined at (i), using corresponding elevation data and multi-angular spectral measurements from a goniometer. We focus on the development of tools that can make Bi-directional Reflectance Distribution Function (BRDF) correction ready for operational use by the community of imaging spectrometry users and developers. The new package of tools called collectively BREFCOR (Bi-directional reflectance correction) is at its beta phase. Here we present the underlying angle-dependant spectral measurements and some sample results from BREFCOR's correction of the CASI and HYMAP imaging spectrometers.

1. RADIOMETRICS

Accounting for the angular positions of illumination (φ_i, θ_i) and sensor (φ_v, θ_v) (see figure 1) we can define directional reflectance $\Delta\rho$ as the ratio of radiance quantities L bound by projected solid angles $\Delta\Omega$:

$$\Delta\rho(\varphi_i, \theta_i, \varphi_v, \theta_v) = \frac{\Delta E_v}{\Delta E_i} = \frac{L_v(\varphi_v, \theta_v)\cdot \Delta\Omega_v}{L_i(\varphi_i, \theta_i)\cdot \Delta\Omega_i}[-] \quad (1)$$
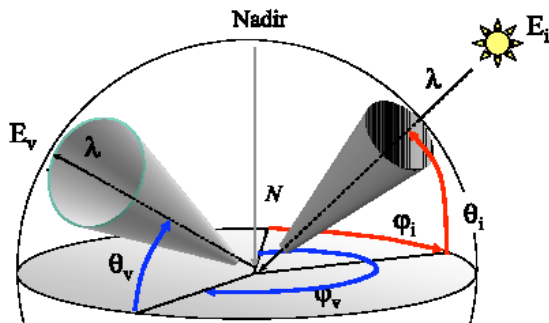

Figure 1. Concept for BRDF

The angular positions of illumination E_i and sensor-viewed radiative flux E_v in figure 1 are defined by azimuth φ and elevation θ

angles. It is already noted by (ii) that the viewed radiance L_v is directly proportional to each of the denominator elements: incoming radiance $L_i(\varphi_i,\theta_i)$ and illumination solid angle $\Delta\Omega_i$ since an increase in irradiance intensity will result in a proportional increase in L_v, and the same is true for increasing the size of $\Delta\Omega_i$. Because of this proportionality, changes to the denominator will not change $\Delta\rho$ and it will stay constant. However, increasing $\Delta\Omega_v$ will increase L_v, changing $\Delta\rho$ as well. Therefore, directional reflectance is dependent on the size of the projected solid angle $\Delta\Omega_v$. In order to achieve a measure free of this dependency $\Delta\rho$ can be normalized by $\Delta\Omega_v$, and so if going to infinitesimal angles we have

$$\text{BRDF}(\varphi_i,\theta_i,\varphi_v,\theta_v,\lambda) =$$

$$\frac{\Delta\rho(\varphi_i,\theta_i,\varphi_v,\theta_v,\lambda)}{\Delta\Omega_v} = \frac{L_v(\varphi_v,\theta_v,\lambda)\cdot\Delta\Omega_v}{L_i(\varphi_i,\theta_i,\lambda)\cdot\Delta\Omega_i\cdot\Delta\Omega_v} =$$

$$\frac{L_v(\varphi_v,\theta_v,\lambda)}{L_i(\varphi_i,\theta_i,\lambda)\cdot\Delta\Omega_i} = \frac{L_v(\varphi_v,\theta_v,\lambda)}{\Delta E_i(\lambda)} \quad [\text{sr}^{-1}] \quad (2)$$

where $\text{BRDF}(\varphi_i,\theta_i,\varphi_v,\theta_v,\lambda)$ is the bi-directional reflectance distribution function for irradiance coming from azimuth and elevation direction φ_i and θ_i respectively and reflected to azimuth and elevation direction φ_v and θ_v respectively, at wavelength λ. BRDF may vary theoretically between 0 and ∞. To estimate irradiance from within the incoming projected solid angle $\Delta\Omega_i$ (so, ΔE_i) we may use any standard Lambertian white reference plate $L_{v,ref}$. However, $\Delta\Omega_v$ is not necessarily the size of $\Delta\Omega_i$, and so this estimate holds only if $\Delta\Omega_i = \Delta\Omega_v$. In such a case, the bi-directional reflectance factor (BRF) is defined by (ii) as:

$$\text{BRF}(\varphi_i,\theta_i,\varphi_v,\theta_v,\lambda) = \frac{L_v(\varphi_v,\theta_v,\lambda)\cdot\Delta\Omega_v}{L_{v,ref}(\varphi_v,\theta_v,\lambda)\cdot\Delta\Omega_v} [-](3)$$

When examining BRF spectra from varying sensor positions it becomes clear that BRF's by themselves do not reveal much in terms of reflectance anisotropy. (iii) suggest emphasizing direction-related reflectance anisotropy with respect to a reference direction, and so to divide each BRF measurement by the nadir BRF measurement, and use the following Anisotropy Factor (ANIF) ratio:

$$\text{ANIF}(\varphi_i,\theta_i,\varphi_v,\theta_v,\lambda) = \frac{\text{BRF}(\varphi_i,\theta_i,\varphi_v,\theta_v,\lambda)}{\text{BRF}(\varphi_i,\theta_i,\varphi_v,\theta_n,\lambda)} [-](4)$$

Therefore ANIF at the nadir point, where $\theta_v=90°$, will equal unity for all wavelengths λ and for all φ_v, a fact that makes ANIF in general, an intuitive reflectance anisotropy measure. All off-nadir ANIF values may vary theoretically between 0 and ∞, but usually remain in the range of 0.5 to 5 at all wavelengths in the spectral range [350nm, 2500nm]. All BRF's (including that at the nadir) can alternatively be referred to the mean bi-hemispherical reflectance (i.e., spectral albedo, BHR) where available. It is therefore convenient to use ANIF (denoted here α for convenience for both kind normalizations) as a starting point for the correction of reflectance anisotropy in hyper-spectral imagery. In order to calculate α's for various materials, wavelengths, and sensor and illumination directions, a set of BRF spectra are required, from a goniometer or from a model. Such datasets are described in the following section.

2.   BRDF FACILITY & DATABASE

The Israeli Goniometric Facility (IGF) (i) allows a mounted spectrometer to measure targets from a maximal distance of about 65cm (to hemisphere centre-point) (figure 2). The sensor is attached firmly to an adjustable arm that can rotate virtually to any point on the hemisphere. This results in a ground IFOV (GIFOV) of about 9cm across at nadir, when using an 8° fore-optic. For each illumination position 113 radiance measurements (L) were taken on the hemisphere with a φ_v resolution of mostly 22.5° (45° interval only near Nadir, at θ_v angles of 70° and 80°) and a θ_v resolution of 10°. These radiance datasets were divided by perfect counterpart radiance datasets of a calibrated white reference (Spectralon®) plate of ASD, assumed to be Lambertian, such that for each sensor position we obtain a BRF.
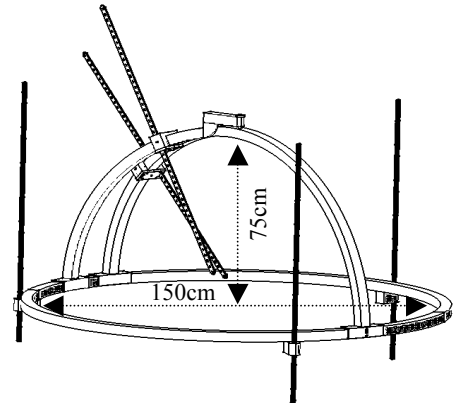
In order to facilitate the use of calculated anisotropy these measurements were projected to a Mercator (rectangular) projection (see figure 3), where 16 φ_v's and 9 θ_v's correspond to the sensor's angular φ_v and θ_v position respectively, and form the X and Y dimensions of a model-image. Within this new layout data gaps at 70° and 80° θ_v positions were filled by inverse-distance interpolation and the nadir measurement was simply replicated 15 times for all nadir φ_v cells (i.e. projected to infinity). Finally data were subset to a θ_v range of [20°, 90°] to avoid outliers at near-horizontal measurements. The resulting datasets formed an estimate of measured reflectance for every 5° for both sensor φ_v and θ_v dimensions (covering 360° in φ_v and [20°, 90°] in θ_v) per illumination angle θ_i.
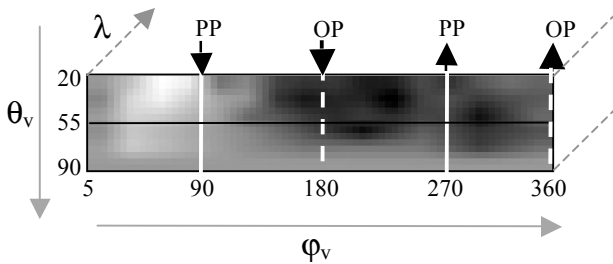

Figure 3. The result of interpolation of spectra to 5° resolution in φ and θ dimensions. The principal plane (PP) and orthogonal plane (OP) are marked with arrows for one illumination angle.

So far, six land-cover classes were measured, representing typical urban land-cover: Soil for (undeveloped) open areas, grass for green areas, asphalt (fresh and weathered) for roads, an arrangement of concrete blocks for pavements and bitumen roofing felt for buildings. All materials were measured with the IGF at laboratory conditions. An example of these results discusses soil in some detail and corresponding analysis. For each BRDF dataset of multiple measurements a set of output figures are produced, to facilitate an intuitive understanding of the library. These include a polar plot at 400nm, a Cartesian surface model fitted to normalized reflectance (ANIF, α) data at 400nm, directional 2D and 3D cross-sections of reflectance ρ, α and the fitted model, and the R^2 correlation coefficient for the overall α cube and its fitted polynomial model. The user can choose whether to normalize by nadir BRF or by albedo spectrum. Example cross-sections of interest of BRF, α and modelled α spectra (explained below) on the principal plane (PP) and the orthogonal plane (OP) are illustrated in figure 4 for soil.

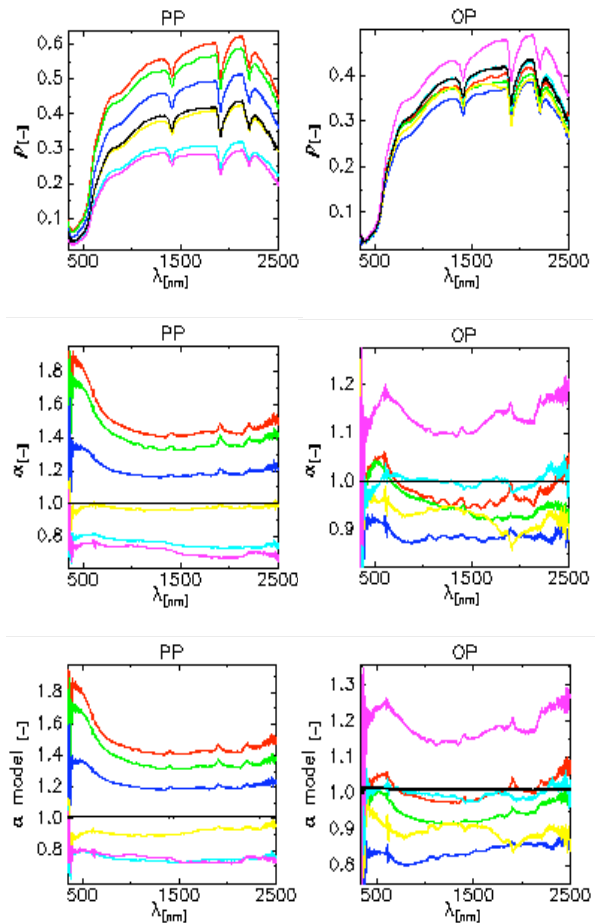Figure 4. A sample of BRF (ρ, top row), nadir normalized ANIF (α, middle row) and modeled ANIF (α model, bottom row) spectra of soil on the principal illumination plane (PP, left column) and orthogonal to illumination plane (OP, right column). Refer also to equations (3, 4) above.

Being the function of illumination and sensor angular positions after interpolation, of wavelength and class, and considering the

three illumination elevation angles currently tested for each of the classes available now, we achieve a total α database size of about $42 \cdot 10^6$ values. The fitted surface layers ("α models") of an α calculated cube are defined in terms of (6th order) polynomial coefficients. This is done for two reasons. First, the similarity of a 6th order polynomial surface fitted to IGF data showed an overall agreement which exceeds $R^2=0.95$ for most materials and for the vast majority of wavelengths in the visible to sort-infrared range. Second, it compresses binary data by a factor of 2.7 (down to 37% of the original size). A surface fitted to each spectral band of the anisotropy calculations cube α may be now used as a general class-specific anisotropy estimate of a land-cover of interest. Although clearly one material sample at the lab will never be representative of all naturally occurring variations of that class, the high similarity of the models to real measurements makes them appropriate replacements and practical estimates for cases where no class-specific anisotropy information is available (being the majority of cases). Coefficients are automatically saved by a dedicated routine to large look-up-tables (LUT's), forming structures that are later convolved with sensor position angles φ'_v and θ'_v, to reconstruct the required α surface (see more at iv for details on that). Currently a total of 18 LUT's of various objects are available in the database.

2.1 Results for soil – an example

A soil sample (Alfisol or "Hamra") was collected from a park in Tel-Aviv. This sandy soil sample exhibited some lumpiness with most blocks of soil having about 0.5cm diameter. An overall uneven texture was observed as seen in figure 5 below. Full analysis of this sample and others are provided in (iv), and a synopsis is given here. Figure 5 reveals that soil has a strong backscatter component. It deviates clearly "backward looks" from "forward looks" to α values being above and below unity (nadir) respectively. This is especially clear on the

Principal plane (PP) and the two diagonal cross-sections, for the whole λ range: [400nm, 2500nm]. While Fe absorption at ~500nm and water absorption features are mainly affecting the PP, clay absorption at 2200nm is mainly affecting the OP. α generally decreases on the PP as illumination elevation θi decrease from 45° to 25° or otherwise increase to 65°. (iii) refer to such a difference as "anisotropy index" (ANIX).

(a)

(b) Anisotropy Factor of alfisol

Illumination $(\phi, \theta) = (90°, 45°)$, $\lambda = 400nm$, Input: alfisol_151008_lns5_v1_090-045.tx

(c) Reflectance of alfisol on the PP
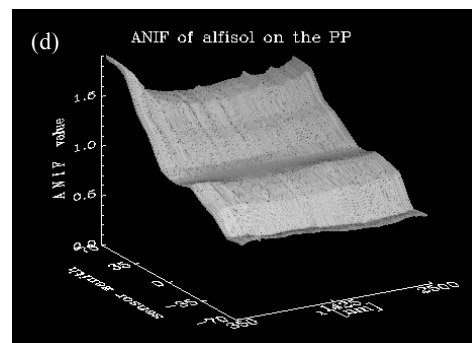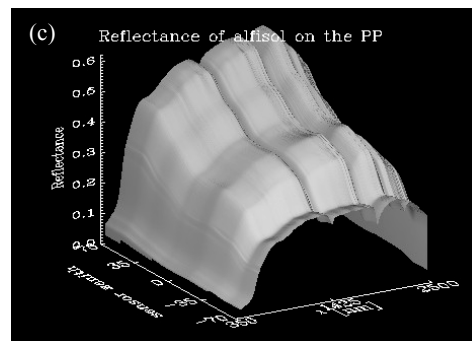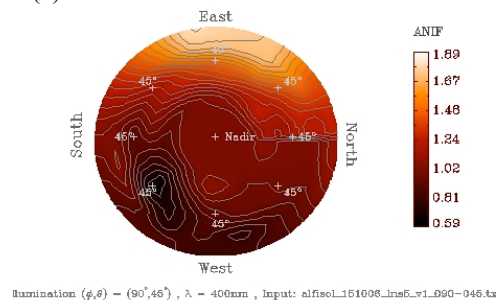
(d) ANIF of alfisol on the PP

Figure 5. (a) Soil sample measurement, (b) polar plot of angular distribution of sample's ANIFs (400nm), with sensor azimuth forming the perimeter and sensor elevation the radius, (c) reflectance of soil on the principal plane (PP) as function of sensor zenith (y axis) and wavelength (x axis), and (d) ANIF of soil on the principal plane (PP), using the same axes as in (c).

3. BREFCOR APPROACHES FOR CORRECTION

The BREFCOR tool case can apply three different workflows for the correction of reflectance anisotropy for flat or rough topography as detailed in (iv, v). Generally it follows a simple logic of three steps: (a) Reconstruction of sensor and illumination angular positions at each image pixel and location of these angles in the BRDF database, (b) match of a corresponding α vector, using global weighting of LUTs and local interpolations when needed, and (c) correction of spectral BRDF by inversion of the matched vector. This is done per image pixel of interest, pre-defined by a classification map, pointing to a specific land-cover.

In the case of rough terrain, the first step requires adjustments of sensor & solar relative angular positions according to rotation in 3D of angles based on local slope and aspect angles (calculation per pixel). The effect is shown in figure 6(a-d) for a case study area in Tel-Aviv, figure 6(f). The second step requires then local weighting and translation of resampled ANIF cubes according to the solar's angular position. To avoid overload of computing such weighting is done of a local angular bounding 2-by-2 spectral subset of the ANIF cube. Extraction of matched spectral ANIF per pixel requires, in most cases, an additional Lagrangian interpolation within the subset. An example result is in figure 6(e). The last step is simply the inversion of spectral ANIF to spectral correction factors and correction of original reflectance by multiplication. If modelled ANIF LUTs are available instead on

calculated ANIF cubes then they are first reconstructed and then serve as regular ANIF cubes in this 3-step process.
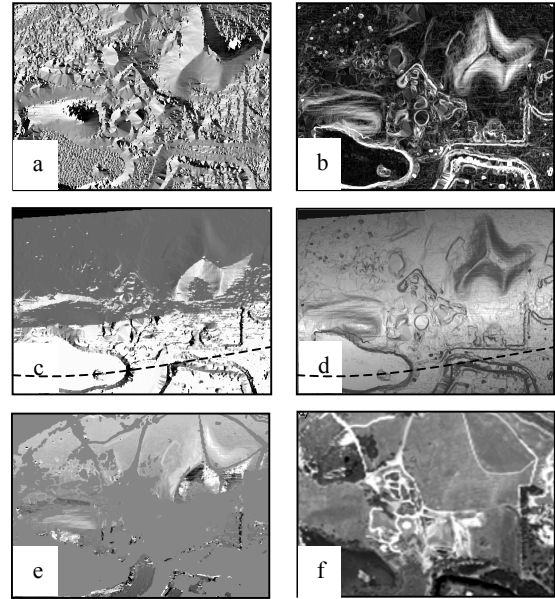

Figure 6. Outputs of major calculation steps during the process of anisotropy correction. (a) aspect map [deg], (b) slope map [deg], (c) map of updated sensor azimuth angles (φ') [deg], (d) map of updated sensor elevation angles (θ') [deg], (e) map of anisotropy value at 681.3nm[-], and (f) an grey-scale copy of an RGB color composite of CASI data of a test site (Tel-Aviv park, Israel). The dashed lines in (c, d) mark the approximated nadir line.

The effect of correction can be visualized by comparing reflectance spectra before and after correction for various locations. However changes are usually minor, and increasing depending on local slope angles. Approximating the correction effect is much clearer if comparing estimates of the actual α spectra before and after correction. This is illustrated in figure 7(a) below for the Tel-Aviv test case using CASI data and in figure 7(b) for a Munich test case using Hymap data. In both cases correction is applied for land-cover class "meadow grass". For this type of land-cover class the correction proves to be effective up to about 1000nm to 1200nm. Beyond that point (i.e. towards longer wavelengths) there seem to be less dependency of ANIF on the angular position of the sensor. Various land-cover classes may

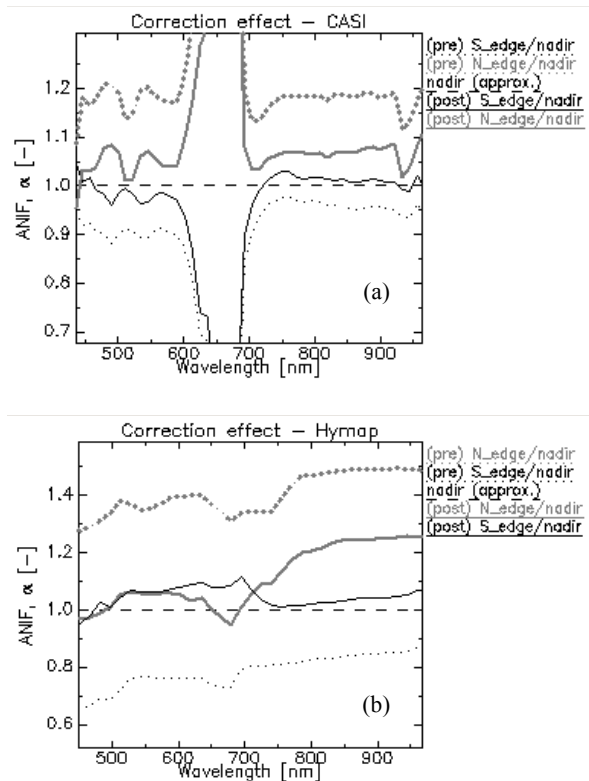have varying spectral sensitivity boundaries in that sense.

Figure 7. (a) CASI, FOV=34°, (b) Hymap, FOV=61°. In both cases "pre" (dotted lines) and "post" (solid lines) refer to the stage of correction, and N (grey thick lines) and S (black thin lines) refer to northern and southern extreme edges of the images respectively. The effect of correction is obvious, with the nadir (dashed) line marking the goal value in both cases, for all wavelengths.

4. CONCLUSIONS

The BREFCOR tool-case is the first effort we know of to operationalize BRDF correction for hyperspectral images in a robust, empirical approach, based on measurements from a goniometer on ancillary data. Test cases for CASI and Hymap images have shown satisfactory results in terms of reflectance anisotropy reduction. This has positive implications on the accuracy of quantitative estimates and mapping applications.

REFERENCES

(i) Feingersh, T, Ben-Dor, E, Filin, S, 2007. Improving anisotropy correction for airborne imaging spectrometers, using a LiDAR DSM and angular spectral measurements. *In: Proceeding of the 5th EARSeL Workshop on Imaging Spectroscopy*, April 2007, Bruges, Belgium.

(ii) Nicodemus, F, E, Richmond, J, C, Hsia, J, J, Ginsberg, I, W, and Limperis, T, 1977. Geometrical considerations and nomenclature for reflectance. Washington, DC: National Bureau of Standards, US Department of Commerce. Washington D.C. 20234. Report no.NBS MN-160.

(iii) Sandmeier S, Müller, C, Hosgood, B, and Andreoli, G, 1998. Physical Mechanisms in Hyperspectral BRDF Data of Grass and Watercress. *Remote Sensing of Environment*, 66: 222-233.

(iv) Feingersh, T, 2007. Aspects of reflectance anisotropy and its propagated influence on analysis of urban dynamics. PhD dissertation, Tel-Aviv University, Israel. 176 pp.

(v) Feingersh, T, Ben-Dor, E, Filin, S, 2009. Correction of reflectance anisotropy: a multi-sensor approach. *International journal of remote sensing* (in press).